ORIGINAL RESEARCH

Sericin-Assisted Green Synthesis of Gold Nanoparticles as Broad-Spectrum Antimicrobial and Biofilm-Disrupting Agents for Therapy of Bacterial Infection

Rui Cai[1,2,*], Qian Cheng[1,3,*], Jiayu Zhao[1], Peirong Zhou[1], Zhaodan Wu[1], Xuemin Ma[1], Yajuan Hu[1], Huiyue Wang[1], Xiaorong Lan[1,2], Jing Zhou[1,4], Gang Tao [1,2]

[1]Luzhou Key Laboratory of Oral & Maxillofacial Reconstruction and Regeneration, The Affiliated Stomatological Hospital, Southwest Medical University, Luzhou, 646000, People's Republic of China; [2]Institute of Stomatology, Southwest Medical University, Luzhou, 646000, People's Republic of China; [3]Department of Orthodontics, The Affiliated Stomatological Hospital, Southwest Medical University, Luzhou, 646000, People's Republic of China; [4]Department of Oral and Maxillofacial Surgery, The Affiliated Stomatological Hospital, Southwest Medical University, Luzhou, 646000, People's Republic of China

*These authors contributed equally to this work

Correspondence: Jing Zhou, Department of Oral and Maxillofacial Surgery, The Affiliated Stomatological Hospital, Southwest Medical University, Luzhou, 646000, People's Republic of China, Email 770384391@qq.com; Gang Tao, Luzhou Key Laboratory of Oral & Maxillofacial Reconstruction and Regeneration, The Affiliated Stomatological Hospital, Southwest Medical University, Luzhou, 646000, People's Republic of China, Email taogang@swmu.edu.cn

Background: Tens of millions of people die from wound infections globally each year, and nearly 80% of tissue infections are associated with bacterial biofilms. However, overuse of antibiotics can lead to bacterial resistance. Therefore, it is critical to develop simple and effective strategies to kill bacteria and remove biofilms.

Methods: The present study used sericin as a reducing and stabilizing agent to synthesize sericin-gold nanoparticles (Ser-Au NPs) and tested its colloidal stability under different pH and salt concentration conditions. Subsequently, functional gold nanocomposites (Ser-Au@MMI) were synthesized by combining Ser-Au NPs with 2-mercapto-1-methylimidazole (MMI). The antimicrobial effect of Ser-Au@MMI was checked by MIC, antimicrobial activity test, and in vitro cytotoxicity was assessed using CCK-8 assay. In vitro anti-biofilm effect was observed by fluorescence microscopy and SEM. Finally, the anti-infective therapeutic efficacy of Ser-Au@MMI was determined in an in vivo rat-infected wound model.

Results: Sericin as a reducing and stabilizing agent to synthesize Ser-Au NPs exhibited excellent colloidal stability under different pH and salt concentration conditions. The TEM, EDS, and XPS analyses confirmed the successful synthesis of Ser-Au@MMI. It exhibited higher antibacterial activity due to the synergistic effect of MMI and AuNP, which can achieve a bactericidal effect by destroying the integrity of bacterial cell walls and structure. In addition, Ser-Au@MMI$_{10}$ (HAuCl$_4$:MMI =1:10) concentration (64 μg/mL) could effectively disrupt biofilms formed by four species of bacteria and kill them, including *P. aeruginosa, B. subtilis, E. coli*, and *S. aureus*, but was not cytotoxic to mouse fibroblasts (L929) cells. Infected wound modeling showed that Ser-Au@MMI$_{10}$ accelerated infected wound healing in vivo.

Conclusion: Ser-Au@MMI nanocomposites are prepared through a facile and environmentally friendly strategy and have the advantages of excellent bactericidal effect and low toxicity, which has the potential for application as a broad-spectrum antimicrobial agent and biofilm disrupting agent in healthcare.

Keywords: antibacterial, gold nanoparticles, green synthesis, wound healing, sericin

Introduction

Wound infections, especially pathogenic bacterial infections, cause millions of deaths yearly.[1,2] Nearly 80% of tissue infections are associated with bacterial biofilms.[3] Biofilms are responsible for most persistent and refractory infections in

humans, such as chronic wounds and refractory infections caused by medical implants.[4–6] Biofilms have a complex structure that encapsulates bacteria in an extracellular polymeric substance (EPS) to protect them from antibiotic penetration and host immune cell attack, making it difficult to eradicate bacteria within biofilms.[7,8] Among the clinical pathogens, *S. aureus* and *P. aeruginosa* tend to form biofilms and are more pathogenic.[9] Infections caused by biofilms are difficult to treat effectively because of their protective effect.[10] If antibiotics are used to eliminate biofilms, the dose required may be more than 1,000 times that of planktonic bacteria.[11,12] More seriously, overuse of antibiotics can lead to bacterial resistance.[13,14] Therefore, developing simple and effective strategies to promote bacterial death and remove biofilms is critical.

The development of nanoscience and nanotechnology has provided promising prospects for applying nanomaterials in anti-biofilm applications.[15–18] Various nanomaterials, including nanosilver[19,20,] zinc oxide,[21] titanium dioxide,[22] and copper oxide,[23] have been investigated and prepared as potential disinfectants for bacterial infections. Li et al reported that nanosilver coated with cationic polymer has a strong anti-biofilm ability.[24] Still, the silver ions released by nanosilver potentially threaten human cells, and lowering the use concentration leads to poor efficacy.[25] Therefore, these nanomaterials' high toxicity or low antimicrobial activity has led to limitations in their use in infected wound healing.[26,27] To increase the local drug concentration while avoiding toxic damage to healthy cells, it is necessary to develop non-toxic or low-toxicity nanomedicine carriers.

Nanoscale precious metals, especially gold, have good stability and biocompatibility, and gold nanoparticles can be easily functionalized by surface ligands, making them an ideal material for drug carriers.[28,29] Jiang et al reported that gold nanoparticles modified with N-heterocyclic molecules and non-antibiotic amines exhibited excellent antibacterial properties.[30] However, functionalized gold nanoparticles are limited in practical applications because toxic reagents such as sodium borohydride and sodium borohydride are used to synthesize gold nanoparticles, which may cause damage to human cells.[31,32] More importantly, gold nanoparticles need good stability for biomedical applications.[33,34] Modifying gold nanoparticles with specific surface ligands, such as surfactants, dendritic polymers, and thiol compounds, effectively prevents aggregation and improves stability.[35,36] However, most of these ligands have the disadvantages of poor biocompatibility and high price.

In recent years, more and more studies have been conducted to synthesize gold nanoparticles by using natural polymers as reducing and stabilizing agents to facilitate the use of toxic substances in the synthesis process and, at the same time, to improve stability and biocompatibility.[37] Natural polymers represented by plant extracts, polysaccharides, and proteins have been widely reported.[38] Sericin secreted by the domestic silkworm is a natural hydrophilic protein with good biocompatibility and biodegradability, which has been widely used in biomaterials and regenerative medicine. Sericin contains 18 amino acids, among which tyrosine residues containing phenolic hydroxyl groups are thought to be used as reducing agents.[39–41] In our previous study, sericin could reduce silver ions in situ to silver nanoparticles and act as a stabilizer to prevent aggregation.[42] Here, gold nanoparticles were synthesized in situ using sericin as a reducing agent and stabilizer. We further explore the possibility of well-stabilized sericin-gold nanoparticles (Ser-Au) as nano-medicine carriers for treating biofilm infections.

In this study, Ser-Au NPs were synthesized utilizing sericin as both a reducing and stabilizing agent (Figure 1A), followed by an examination of the colloidal stability of Ser-Au NPs under varying pH and salt concentrations. Subsequently, Ser-Au NPs were employed as a delivery system for the loading of a small drug molecule, 2-mercapto-1-methylimidazole (MMI) (Figure 1B), to investigate the biocompatibility and antimicrobial efficacy of drug-loaded gold nanoparticles against Gram-negative (*E. coli* and *P. aeruginosa*) and Gram-positive (*S. aureus* and *B. subtilis*) bacterial strains. In addition, Ser-Au @MMI was explored in vitro for bacterial biofilm disruption effect and in vivo for pro-infectious wound healing ability (Figure 1C and D). In conclusion, we synthesized Ser-Au@MMI with anti-biofilm and good compatibility in a simple, economical, and facile way, which provides a prospect for synthesizing optimal AuNP antibacterial materials.

Materials and Method
Materials
HAuCl$_4$·4H$_2$O was purchased from China National Pharmaceutical Group Corporation (Beijing, China). Silkworm cocoons were purchased from the Seri Cultural Research Institute of Jiangsu Province, China. 2-mercapto-1-methylimidazole (MMI,
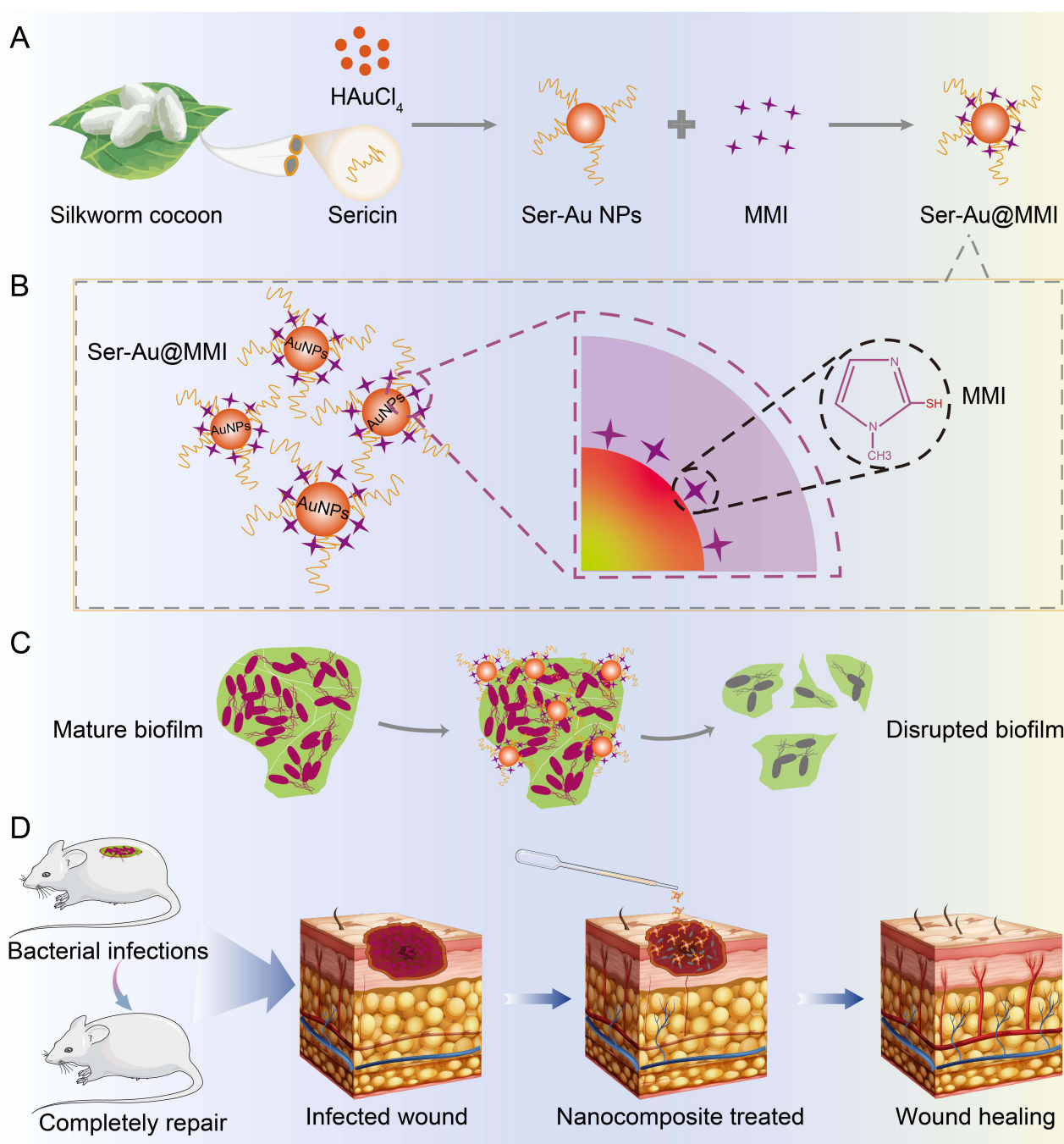
Figure 1 Schematic representation of the synthesis process of Ser-Au@MMI nanocomposite and its potential application in wound healing. (**A** and **B**) Schematic illustration of the preparation process of Ser-Au@MMI nanocomposites and (**C** and **D**) their disruption of biofilm and the promotion of infected wound healing.

98%) was obtained from Aladdin (Shanghai, China). Cell counting kit-8 (CCK-8) was purchased from Beyotime (Beijing, China). LIVE/DEAD BacLight bacterial viability kit was purchased from Thermo Fisher Scientific (MA, USA). Standard strains of *Staphylococcus aureus* (*S. aureus*, ATCC25923), *Escherichia coli* (*E. coli*, ATCC25922), *Pseudomonas aeruginosa* (*P. aeruginosa*, ATCC27853), and *Bacillus subtilis* (*B. subtilis*, ATCC9372) were obtained from the China General Microbiological Culture Collection Center. Cell strains of mouse fibroblasts (L929) cell lines were bought from China Infrastructure of Cell Line Resources. All other chemicals are analytical and suitable for direct use.

Isolation of Sericin

Consistent with previous reports, we used heat and alkaline degumming methods to extract sericin from silkworm cocoons.[43] Briefly, 5 g of silkworm cocoons were cut into small pieces and washed thrice with deionized water. Then, the small pieces of silkworm cocoons were immersed in sodium carbonate solution (300 mL, 0.02 M) and boiled for 60 min. Subsequently, silk fibroin was removed. The raw solution was dialyzed with (MW: 14 kDa) deionized water for 2 days to remove sodium carbonate and then lyophilized to obtain sericin powder.

Synthesis of Ser-Au NPs

The sericin-coated gold nanoparticles (Ser-Au) are synthesized by reducing the $HAuCl_4$ using sericin as a reducing agent. First, 0.1 g of sericin was dissolved in 10 mL ultrapure water. Then, the sericin solution was quickly added to 100 μL of $HAuCl_4 \cdot 4H_2O$ (1 mm), and the mixed solution was heated and boiled at different times with constant stirring (MS-H280-Pro, China). The formation of Ser-Au NPs was analyzed by UV-Vis spectroscopy (TU-1810, Shanghai, China) in the wavelength range of 200 to 1000 nm.

Colloidal Stabilities of Ser-Au NPs

Gold nanoparticles (Au NPs) synthesized by reduced $HAuCl_4$ by sodium citrate were used as a control.[29] Au NPs and Ser-Au NPs were added to 1.5-fold Tris–HCl-buffered synthetic body fluid (SBF) solutions (volume ratio, 1:2) and detected by UV-vis spectroscopy. The Ser-Au NPs were added to 1-fold salt solutions (volume ratio, 1:1) at pH 7.4, and UV-vis determined the stability of the Ser-Au NPs concerning various salt concentrations. The Ser-Au NPs were added to 20 mm tris (hydroxymethyl) aminomethane–2-(N-morpholino) ethanesulfonic acid (Tris–MES) or 20 mm phosphate buffer solution (PBS) at pH 3 to 11 (volume ratio, 1:1), and UV-vis determined the pH stability of the Ser-Au NPs. The Ser-Au NPs were treated at different temperatures for 7 days, and UV-vis detected their stability.

Synthesis of 2-Mercapto-1-Methylimidazole-Capped Ser-Au (Ser-Au@MMI) Nanocomposites

The 0.1 g of sericin was dissolved in 10 mL ultrapure water, and then 100 μL of $HAuCl_4 \cdot 4H_2O$ (1 mm) was quickly added to the solution and boiled for 14 min. After cooling, MMI was added to the mixed solution according to different initial molar ratios ($HAuCl_4$:MMI = 1:1, 1:5, 1:10, and 1:20) and stirred for 10 min to obtain Ser-Au@MMI$_1$, Ser-Au@MMI$_5$, Ser-Au@MMI$_{10}$, and Ser-Au@MMI$_{20}$ nanocomposites, respectively. Then, the nanocomplexes were to be filtered with a 0.22 μm filter (Millipore, USA) and stored at 4°C.

Characterization of Ser-Au@MMI Nanocomposites

The morphologies of Ser-Au NPs and Ser-Au@MMI composites were observed using a JEM-2100 transmission electron microscopy (JEOL, Japan).

The composition and distribution of elements in Ser-Au@MMI composites were examined using an X-ray energy dispersive spectroscopy (EDS) detector. The specific elements and chemical state were analyzed by X-ray photoelectron spectroscopy (XPS, Shimadzu Kratos AXIS Ultra DLD, Japan).

Antibacterial Activity Test by MIC

We used the micro-broth dilution method to determine the minimum inhibitory concentration (MIC) of nanocomposites according to previously reported.[44] The nutrient broth was first added to 96 wells with 50 μL per well, and then 50 μL of nanocomposites with different concentrations (1, 2, 4, 8, 16, 32, 64, and 128 μg/mL) were added to each well. After mixing, 10 μL of bacteria (concentration: 1×10^6 CFU/mL) were added into each well. The wells were then incubated at 37°C for 24 h. The minimum drug concentration that does not cause turbidity in the bacterial suspension is the MIC.

Antibacterial Activity Test by SEM Observation

The bacterial suspension (1×10^6 CFU/mL) was co-cultured with Ser-Au@MMI nanocomposites (32 μg/mL) for 2 h. The treated bacteria were collected by centrifugation (Thermo Fresco 17, USA) and washed three times with PBS. Untreated bacteria served as controls. Bacterial samples were fixed with 2.5% glutaraldehyde for 12 h and washed three times with PBS. It was then dehydrated with 50%, 70%, 80%, 90%, 95%, and 100% ethanol solution for 15 min and lyophilized. Finally, the samples were disposed of by metal spraying and observed by SEM (Hitachi SU3500, Japan).

Cytotoxicity Assay

The cytotoxicity of Ser-Au@MMI nanocomposites was assessed by Cell counting kit-8 (CCK-8) assay. Cells were cultured in Dulbecco's modified Eagle medium (DMEM) containing 10% fetal bovine serum and 1% Streptomycin/ Penicillin at 5% CO_2 and 37°C. L929 cells (1×10^4 cells/well) were added to a 96-well plate, and then different concentrations of nanocomposites were added to each well and cultured for 24 h. CCK-8 solution (10 μL) was added to each well and incubated at 37°C for 1.5 h. The absorbance of each well was measured at 450 nm using a microplate reader (TECAN Infinite M200PRO, China).

Anti-Biofilm Effects by Fluorescence Microscope Observation

Bacteria were diluted to 1×10^8 CFU/mL using fresh tryptic soy broth medium (TSB), and the bacterial suspension (500 μL) was added to a 24-well plate and incubated for 48 h at 37°C. The TSB medium was replaced every day. Then, the medium was aspirated and gently washed three times with PBS to remove the planktonic bacteria and added to 500 μL of fresh medium with Ser-Au@MMI$_{10}$ nanocomposites or PBS, respectively. After 5 h, the wells were washed three times with PBS to remove the planktonic bacteria, added LIVE/DEAD bacterial staining reagents, and then observed by fluorescence microscopy (Leica, DMi8, Germany).

Anti-Biofilm Effects by SEM Observation

Bacteria were cultured using the above method to form biofilms on a glass sheet and then treated with Ser-Au@MMI$_{10}$ nanocomposites. Free bacteria were washed away with PBS. The treated bacterial samples were fixed with glutaraldehyde (2.5%, v/v) overnight and then dehydrated and lyophilized using a range of ethanol solutions (50%, 70%, 80%, 90%, 95%, and 100%, v/v). Finally, the samples were disposed of by metal spraying and observed by SEM (Hitachi SU3500, Japan).

In Vivo Infected Wound Model in Rat

Animal experiments were approved by the Ethics Committee of Southwest Medical University (Approval No.: 20 240 904–003). The experiments were performed in accordance with the Ethics Committee of Southwest Medical University and followed all aspects of the Guidelines for the Care and Use of Laboratory Animals. Male Sprague Dawley (SD) rats (200–220 g, 7–8 weeks) were anesthetized, and a full-thickness circular wound with a diameter of 10 mm was made on the back. The wound was infected with *S. aureus* or *P. aeruginosa* (100 μL, 1×10^7 CFU/mL). After 2 h, 100 μL of Ser-Au@MMI$_{10}$ (64 μg/mL) or PBS was smeared on the wounds of the treatment group and control group once a day. The wound area was photographed with a digital camera to document healing, and ImageJ was used to quantify the average wound area. Wound closure (WC) was determined by the following equation:[45]

$$WC\% = (S0 - St)/S0 \times 100\%$$

Where S0 is the wound area on day 0, and St is the wound area on days 4, 8, or 12.

Histological Analysis

Rat wound skin tissues from days 4, 8, and 12 were collected and placed in 4% (v/v) paraformaldehyde solution. Then, they were embedded with paraffin and stained with hematoxylin and eosin (H&E). Finally, a digital pathology slide scanner (KF-PRO-002, China) was used for imaging observation.

Statistical Analysis

All the quantified data were presented as the mean ± standard deviation. The statistical significance was analyzed using the Student's *t*-test. In all cases, $p < 0.05$ was considered statistically different.

Results and Discussion

Synthesis and Characterization of Ser-Au NPs

As a natural protein, sericin contains 18 amino acids, including tyrosine, tryptophan, and phenylalanine, which are amino acids with phenyl rings and have exceptional UV absorption. As shown in Figure 2A, the absorption peaks at 227 nm and 275 nm were observed in the UV–Vis spectra of sericin solution, which attributed to the absorption of aromatic amino acids and peptide bonds.[46] The surface plasmon resonance band of typical Au NPs was observed at 525 nm in the UV–Vis spectra of Ser-Au NPs, which indicated the successful synthesis of Ser-Au NPs[47] (Figure 2B and C). The results of reaction kinetics showed that the absorbance at 525 nm increased with increasing reaction time and reached a plateau after 14 min (Figure 2D–F). It was also observed that the color of the solution turned into a typical red colloidal AuNP solution with the increase in reaction time, and no further change was observed after 14 min (Figure 2G), indicating that the reaction was completed.

Stabilities of Ser-Au NPs

Good stability under environmental conditions such as physiological solutions, high salt concentrations, and extreme pH values is a prerequisite for gold nanoparticles in biological and medical applications.[34] Simulated body fluid (SBF) is very similar to the ionic composition of human plasma.[48] Ser-Au NPs and Au NPs synthesized with sodium citrate were
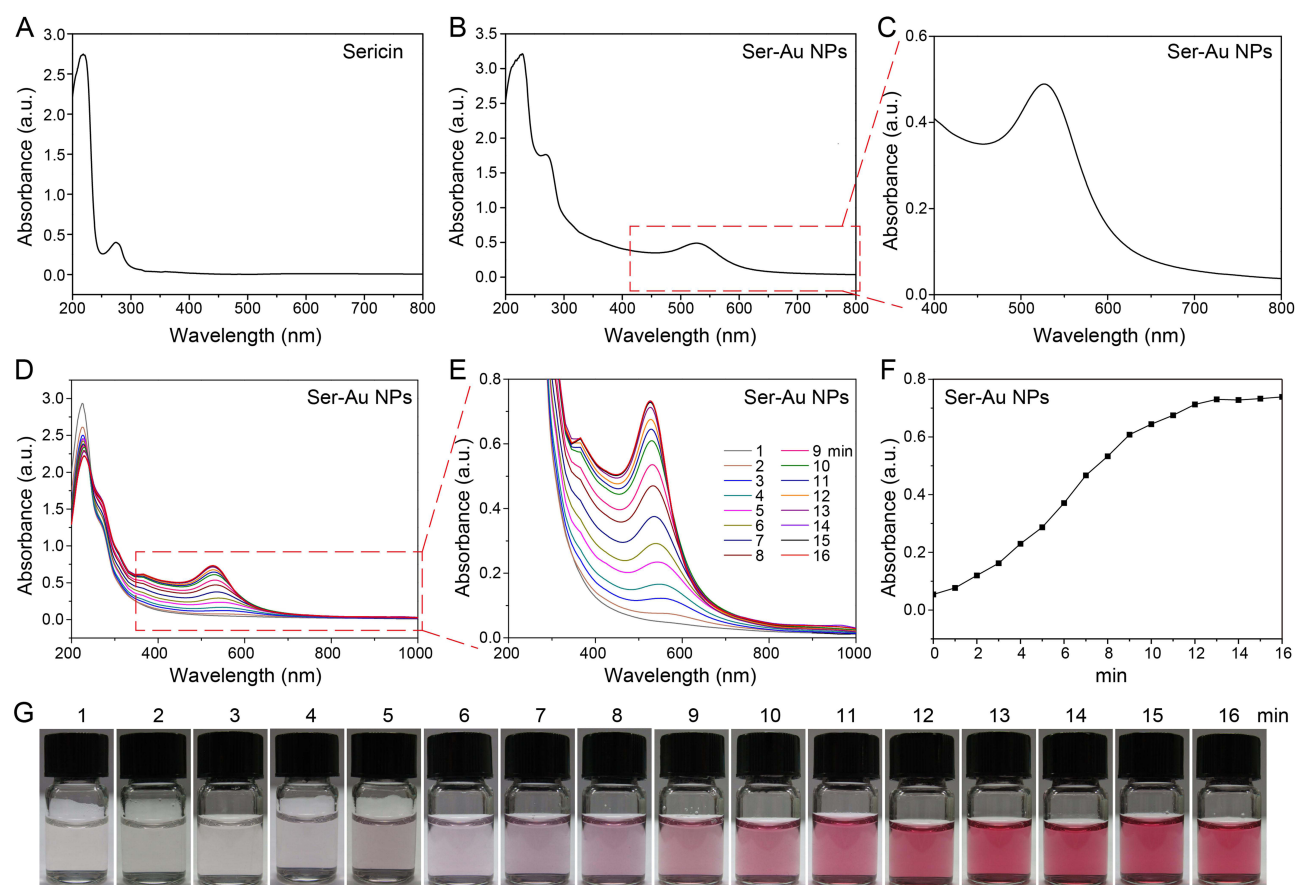

Figure 2 Characterization of Ser-Au NPs. UV–Vis spectra of (**A**) sericin and (**B** and **C**) Ser-Au NPs. (**D** and **E**) Time-resolved UV-Vis spectra and (**F**) time-dependent absorbance at 525 nm after 0–16 min reaction of sericin and HAuCl₄. (**G**) Optical images of Ser-Au NPs.

incubated in SBF solution for 48 h to test their stability. The UV–Vis results showed that the absorption peaks of Ser-Au NPs at 525 nm were unchanged, while those of Au NPs disappeared (Figure 3A–C). This result implied that Ser-Au NPs have good stability in complex biological systems.

It is crucial to ensure that nanoparticles can be stored if they are to be used for biological and medical applications. The nanomaterials were placed in 25°C and 37°C environments for 7 days, and the UV-Vis absorption spectra showed no change in the intensity and position of the absorption peak at 525 nm for Ser-Au NPs (Figure 3D). This result indicated that Ser-Au NPs have excellent temperature stability and can be stored for a long time.

MES-Tris buffer was used to reduce the effect of salt ions, and the impact of pH on the stability of Ser-Au NPs was investigated. Figure S1A shows the UV-Vis absorption spectra of Ser-Au NPs at different pH conditions, and there was no change in the intensity and position of the absorption peak at 525 nm for Ser-Au NPs in the pH range from 3 to 11. A similar phenomenon was observed in phosphate buffer with pH values ranging from 3 to 11 (Figure S1B), indicating that Ser-Au NPs have excellent pH stability.

The effect of salt concentration on the stability of Au NP was further analyzed. The results of UV-visible spectroscopy showed no significant change in the absorption characteristic peaks of Ser-Au NP when the final concentration of NaCl was 15–1000 mm (Figure S1C). Metal ions such as K^+, Ca^{2+}, and Mg^{2+} affect the rheological properties of proteins;[49] therefore, we also investigated their effects on the stability of Ser-Au NPs. The results of
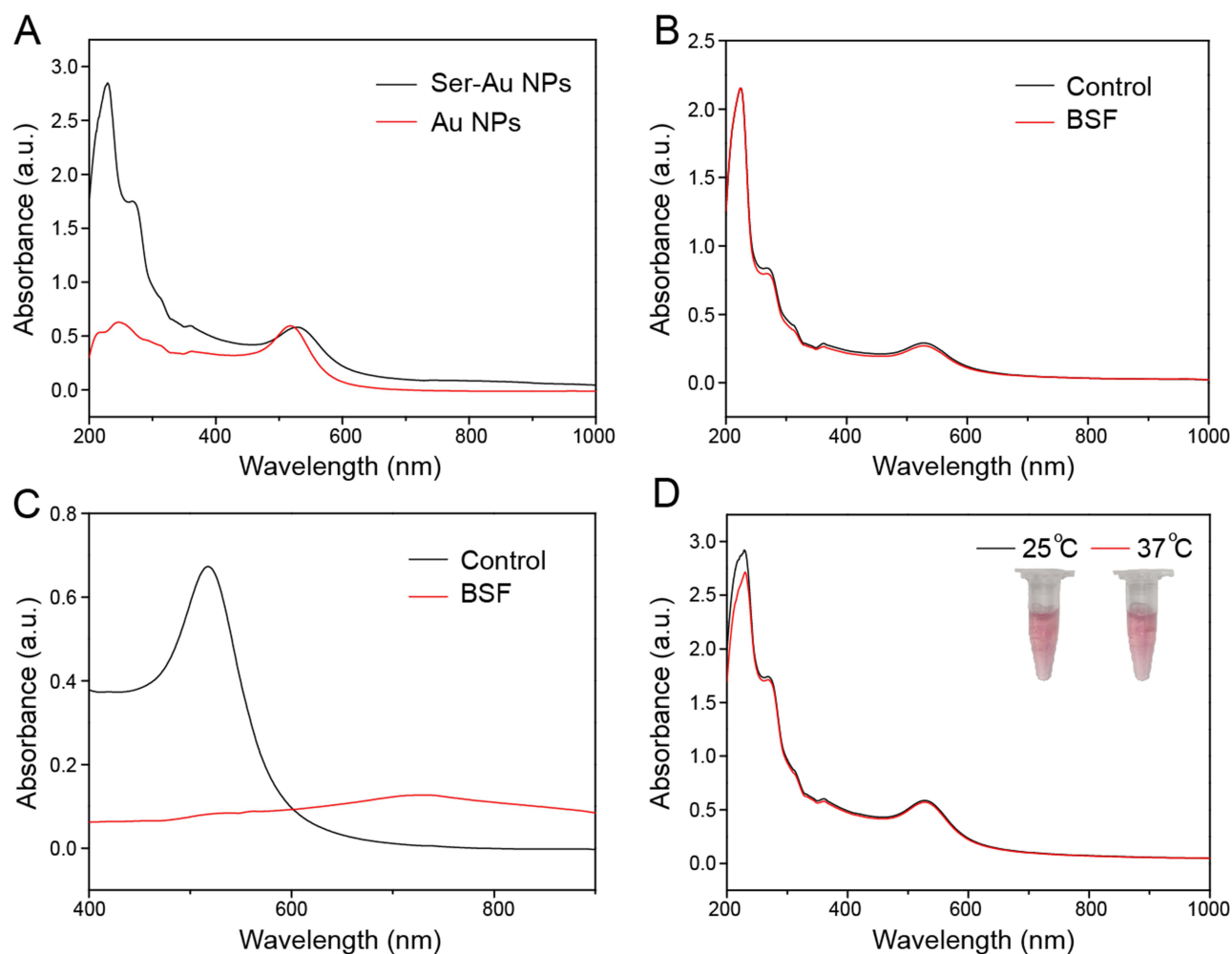

Figure 3 (A) UV–Vis spectra of Ser-Au NPs and sodium citrate-synthesized gold nanoparticles (Au NPs). UV–Vis spectra of (B) Ser-Au NPs and (C) Au NPs in SBF solution. (D) UV–Vis spectra of Ser-Au NPs in 25°C and 37°C.

UV-visible spectroscopy showed that the characteristic peaks of Ser-Au absorption remained stable at high concentrations of metal ions (Figure S1D-F). Increasing electrostatic repulsion and spatial site resistance on the surface of NPs can significantly improve the stability of NPs.[47] In our system, sericin has a random helical conformation.[50] Encapsulation on the surface of Au NPs increases the spatial potential resistance of the particles. Therefore, the spatial effect of sericin has excellent stability to Ser-Au NPs.

Synthesis and Characterization of Ser-Au@MMI

We prepared an antibiotic MMI-capped Au nanocomposites by reducing $HAuCl_4$ using sericin and adding MMI. TEM observations revealed that Ser-Au and Ser-Au@MMI were spherical and well dispersed. A high-resolution transmission electron microscope (HRTEM) showed that the lattice spacing of the nanoparticles is 0.235 nm, which corresponded to the (111) plane of gold.[51] The average particle sizes of Ser-Au and Ser-Au@MMI were 10.07 nm and 8.79 nm, respectively (Figure 4A), indicating that the introduction of MMI can reduce the size of Au NPs.[52]
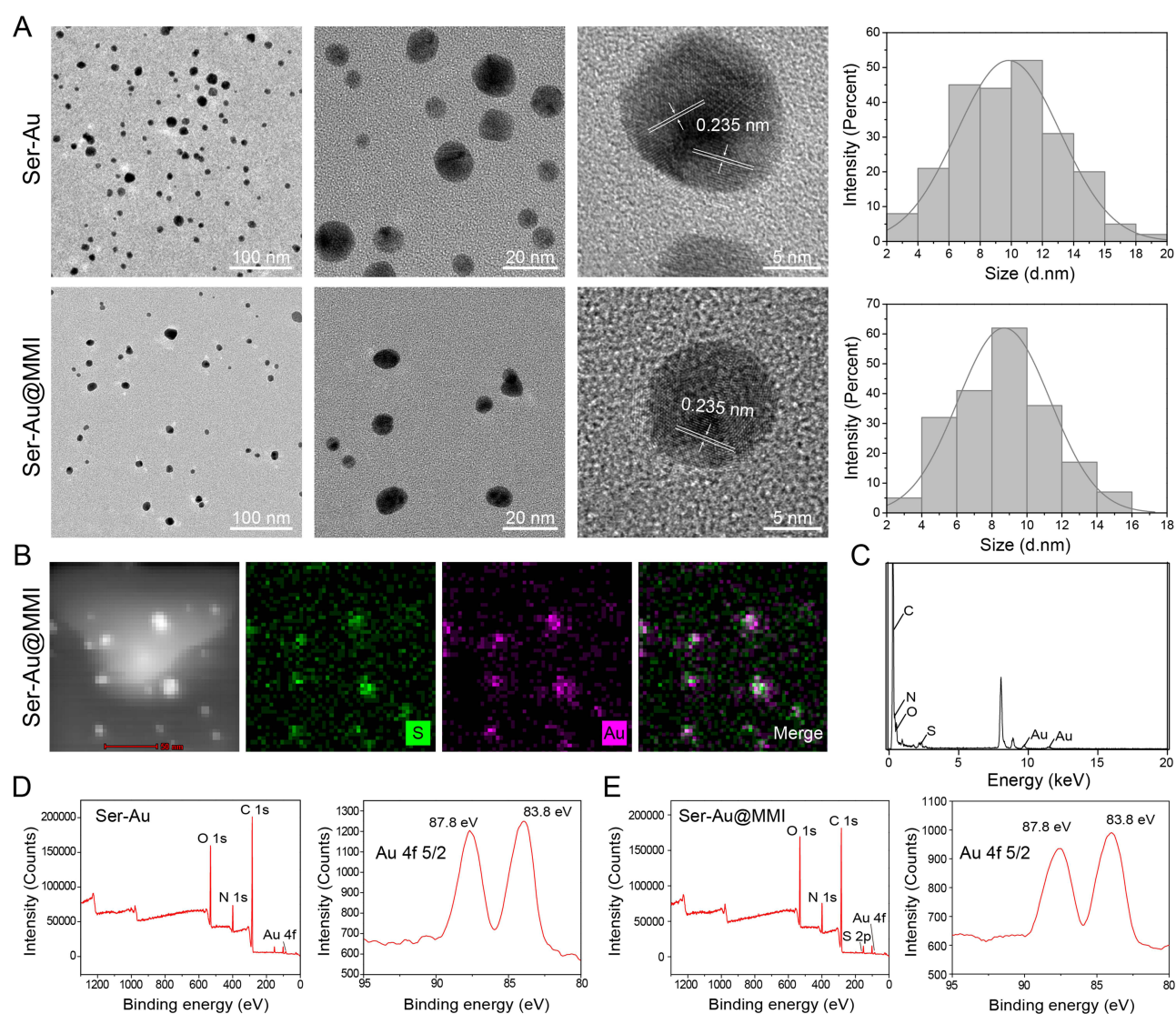

Figure 4 Characterization of Ser-Au@MMI nanocomposites. (**A**) TEM images and the corresponding particle size distribution of Ser-Au and Ser-Au@MMI$_{10}$, respectively. (**B**) Chemical mapping of the Ser-Au@MMI$_{10}$ nanocomposite by HAADF-STEM. (**C**) Energy dispersive spectrometer analysis of Ser-Au@MMI$_{10}$. XPS spectra of (**D**) Ser-Au and (**E**) Ser-Au@MMI$_{10}$.

High-angle annular dark field scanning transmission electron microscopy (HAADF-STEM) was used to label the elements of Ser-Au@MMI and thus illustrate the structure of Ser-Au@MMI nanocomposites. Figure 4B shows the mapping of S (green) and Au (purple) with overlapping positions of S and Au, indicating that the MMI molecules were successfully functionalized on the surface of the Au cores through the interaction of sulfhydryl groups (-SH) with the Au NPs. XPS was used to characterize Se-Au@MMI's elemental compositions and valence state of Au. As shown in Figure 4C, peaks of C, N, O, S, and Au 4f are observed, where C, O, and N are the major elements of the sericin. Further analysis revealed that the binding energies of Au $4f_{5/2}$ and Au $4f_{7/2}$ were 87.8 eV and 83.8 eV (Figure 4D and E), respectively, which were common for metallic Au.[53] These results indicated that Se-Au@MMI was successfully synthesized.

Antibacterial Activity of Ser-Au@MMI

We determined the antimicrobial activity of Ser-Au@MMI based on the MIC value assay using Gram-negative (*E. coli* and *P. aeruginosa*) and Gram-positive (*S. aureus* and *B. subtilis*) bacteria as microbial models. As shown in Figure 5, the antibacterial ability of Ser-Au@MMI$_{20}$ was significantly more potent than that of Ser-Au@MMI$_5$ and Ser-Au@MMI$_{10}$ at the same concentration, and the MIC value decreased from 32 μg/mL to 2 μg/mL. The molar ratio between HAuCl$_4$ and MMI increased from 1:1 to 1:20, allowing more ligands (MMI) to bind to Au NPs, resulting in more potent antibacterial effects. Additionally, the introduction of the MMI molecule suppressed the size of Au NPs, which may have increased their surface area and enhanced their surface energy.[52]

Antibacterial Mechanism of Ser-Au@MMI

After Ser-Au@MMI (32 μg/mL) treatment of Gram-negative (*E. coli* and *P. aeruginosa*) and Gram-positive (*S. aureus* and *B. subtilis*) bacteria, the morphology of the bacteria was observed by SEM to elucidate the antimicrobial mechanism of the nanocomposites. As shown in Figure 6A, the untreated bacteria were rod- and round-shaped with smooth and intact cell walls. After being treated with Ser-Au@MMI, all bacterial cell walls appeared wrinkled with fold and breakage, and the impairment of the bacterial cell wall integrity became more and more severe as the molar ratio of HAuCl$_4$ between MMI increased from 1:1 to 1:20.

TEM was further utilized to observe the morphology of bacteria before and after Ser-Au@MMI treatment. Gram-negative bacterium of *P. aeruginosa* and Gram-positive bacterium of *S. aureus* are common infectious bacteria in hospitals and were used as model bacteria. The untreated bacteria showed intact bacterial morphology and clear cell walls. However, after Ser-Au@MMI$_{10}$ treatment, the bacteria showed partial membrane lysis (Figure 6B). These results suggested that the antibacterial activity of Ser-Au@MMI was attained by destroying the cell walls as well as membranes and damaging the structural integrity of bacteria, ultimately leading to bacterial death.

Cytotoxicity Assays of Ser-Au@MMI

Low cytotoxicity is an essential prerequisite for using biomaterials in medical applications; therefore, in this study, we evaluated the cytotoxicity of Ser-Au@MMI on L929 cells using CCK-8 analysis. As shown in Figure S2, the cell survival was 95% after treatment with Ser-Au@MMI$_1$, Ser-Au@MMI$_5$, and Ser-Au@MMI$_{10}$ (concentration ≤ 128 μg/mL) for 24 h. When the concentration of Ser-Au@MMI$_{20}$ was greater than 32 μg/mL, it showed significant cytotoxicity against L929 cells. The toxicity of Ser-Au@MMI$_{20}$ at high concentrations (64 μg/mL and 128 μg/mL) may result from free MMI molecules that fail to bind to Ser-Au NPs. Combined with the results of antimicrobial experiments, Ser-Au@MMI$_{10}$ (64 μg/mL) nanocomposite was selected as the optimal antimicrobial material.

Anti-Biofilm Activity of Ser-Au@MMI

Microbial biofilms are resistant to antimicrobial agents and the immune system, and the chronic infections caused by biofilms represent a significant clinical challenge.[2,54] Therefore, we investigated whether Ser-Au@MMI could eliminate formed biofilms. The SEM results showed that the biofilm structures of four bacteria were significantly structurally disrupted after Ser-Au@MMI$_{10}$ (64 μg/mL) treatment (Figure 7A), and most of the bacteria were killed.
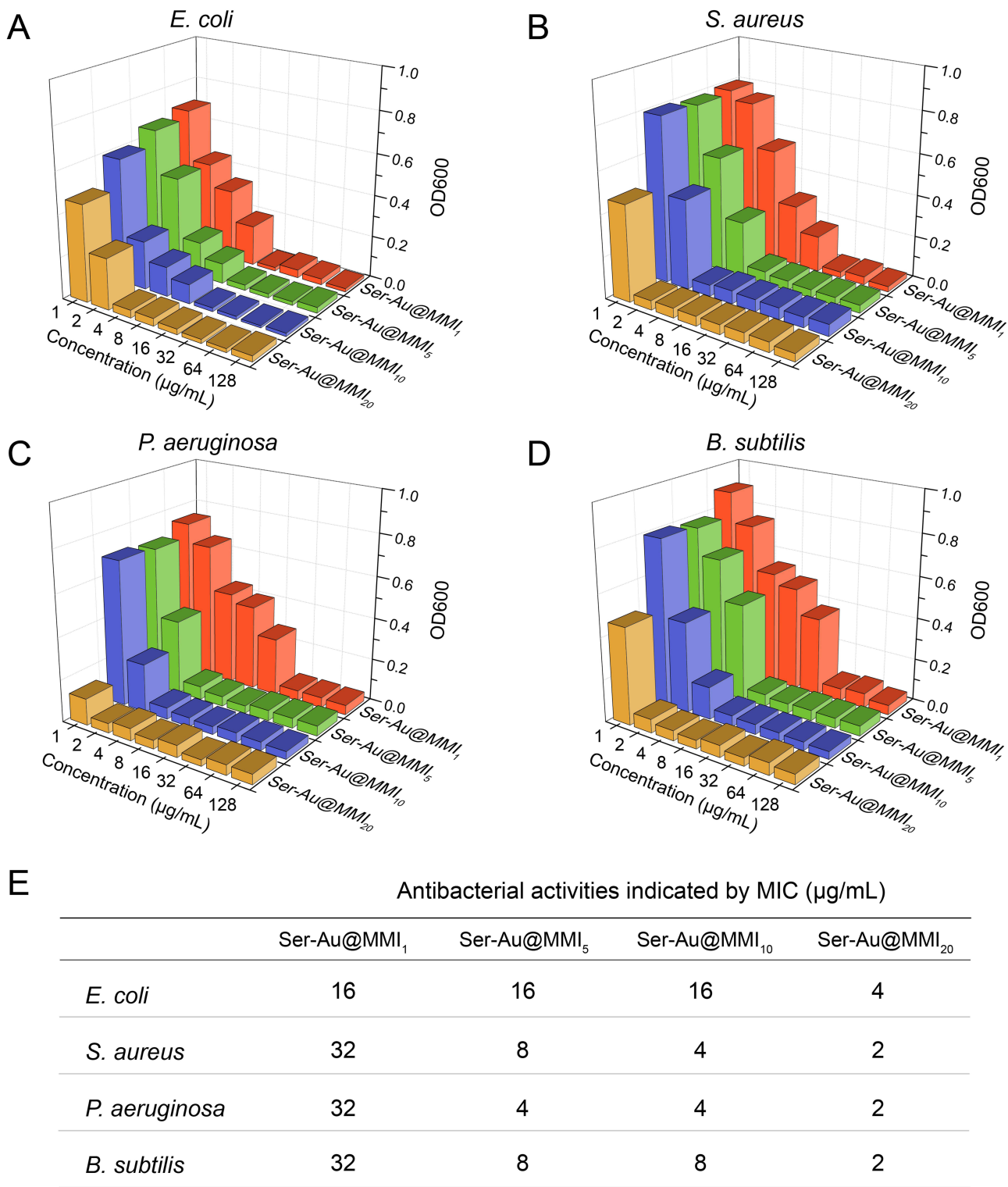
Figure 5 Antibacterial effect of different ratios of Se-Au@MMI for (**A**) *E. coli*, (**B**) *S. aureus*, (**C**) *P. aeruginosa*, and (**D**) *B. subtilis*. (**E**) MIC of Se-Au@MMI against bacterial strains.
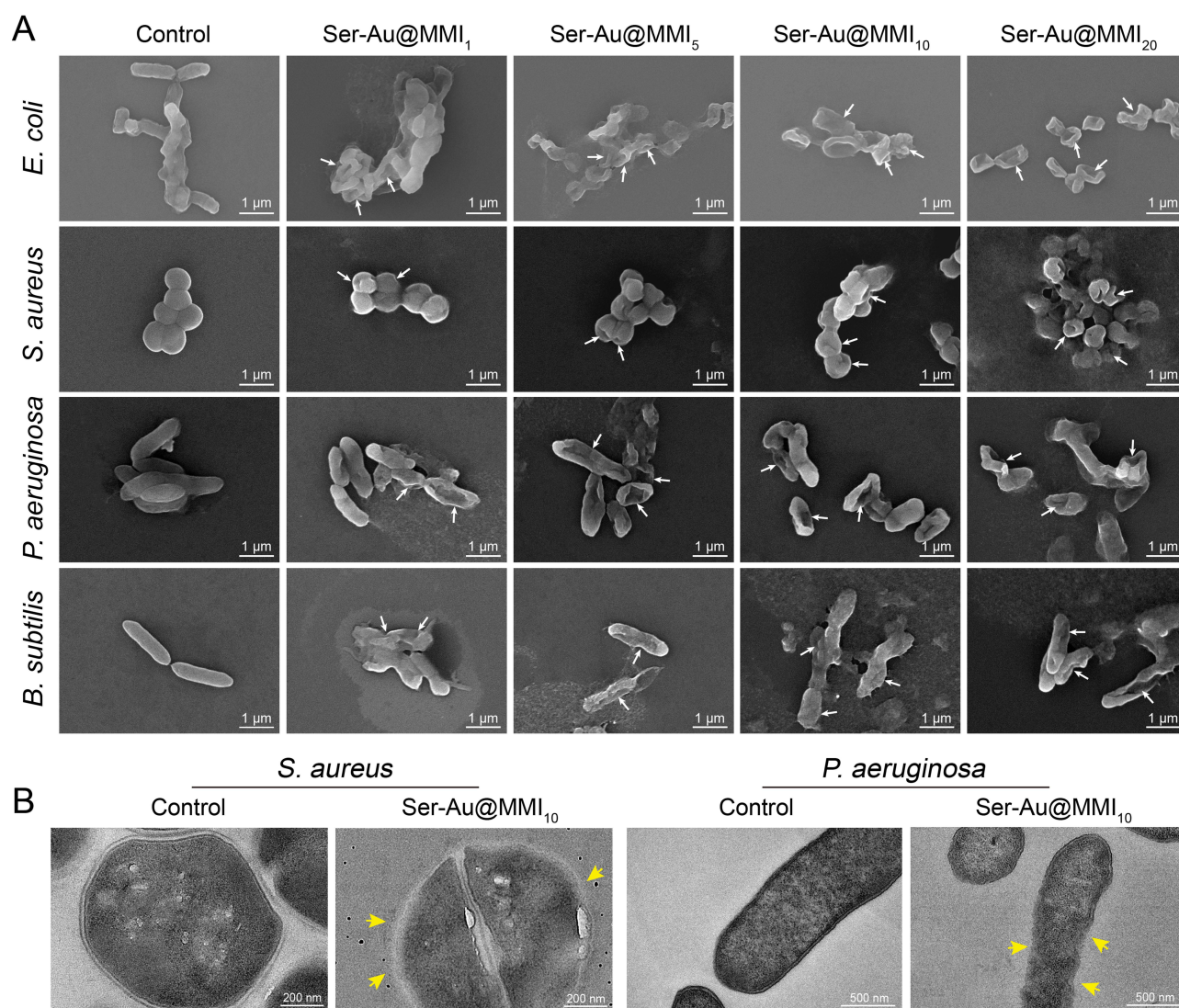
Figure 6 Morphological observation of *E. coli, S. aureus, P. aeruginosa*, and *B. subtilis* before and after treatment of Ser-Au@MMI. (**A**) SEM images of bacteria before and after treatment of Ser-Au@MMI. (**B**) TEM images of *P. aeruginosa* and *S. aureus* before and after treatment of Ser-Au@MMI$_{10}$.

Biofilm damage by Ser-Au@MMI$_{10}$ was further assessed using live/dead staining analysis. Live bacteria with intact cell membranes are labeled green, and dead bacteria with disrupted cell membranes are shown in red. As shown in Figure 7B, the green fluorescence of the four bacteria was significantly reduced, and the red fluorescence was significantly increased after treatment with Ser-Au@MMI$_{10}$ (64 μg/mL). This result indicates that Ser-Au@MMI$_{10}$ can effectively kill bacteria in biofilms and disrupt the biofilm, which agrees with the results of SEM.

In Vivo Wound Healing Studies and Histologic Analysis

To investigate the function of Ser-Au@MMI$_{10}$ (64 μg/mL) in vivo, we evaluated its effect on wound healing in rat models infected with *S. aureus* or *P. aeruginosa* (Figure 8A). Two wounds were created on each rat: the control group and the Ser-Au@MMI$_{10}$-treated group, and the wounds were photographed on days 0, 4, 8, and 12 to examine the wound healing status. As shown in Figure 8B and C, the Ser-Au@MMI$_{10}$-treated group had more minor wounds than the control group after 8 days, with a wound healing rate of 90%. After 12 days of treatment, the scars in the Ser-Au@MMI$_{10}$ group were almost completely healed. Statistical analysis of the wound healing rate showed that the wound healing effect of the Ser-Au@MMI$_{10}$-treated group was significantly better than that of the control group (Figure 8D).
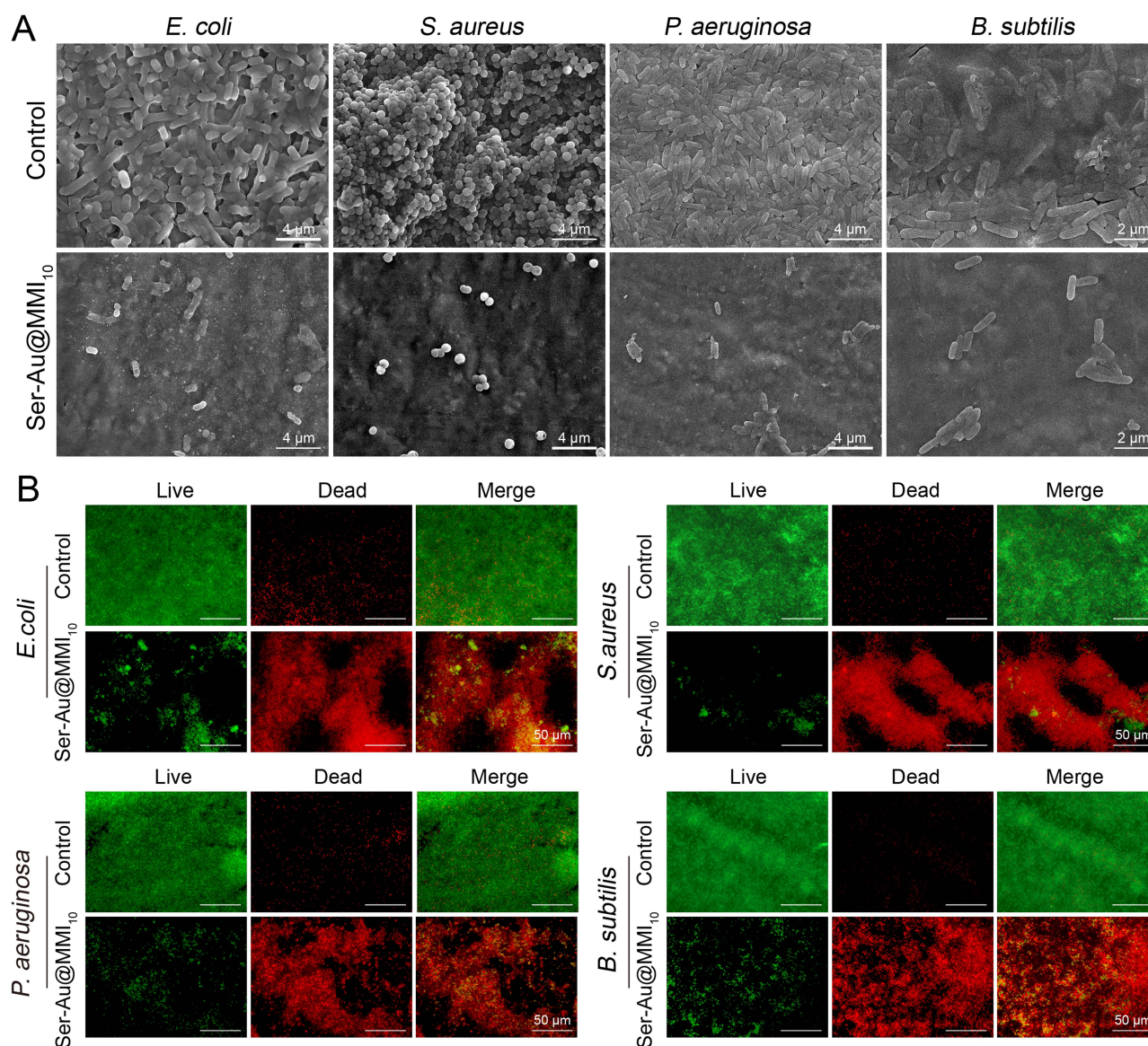
Figure 7 Morphological observation of biofilm of *E. coli, S. aureus, P. aeruginosa*, and *B. subtilis* before and after treatment of Ser-Au@MMI$_{10}$. (**A**) SEM images. (**B**) Live/dead staining assay.

To assess the wound healing process, tissue fixation around the infected wounds was collected and evaluated histologically on days 4, 8, and 12, respectively. In the *S. aureus* infection model (Figure 9A), the tissues of the PBS-treated group showed many inflammatory cells and epithelial loss on days 4 and 8, indicating a severe inflammatory response. However, few inflammatory cells were observed in the tissues of the group treated with Ser-Au@MMI$_{10}$, indicating that Ser-Au@MMI$_{10}$ nanocomposites have good antimicrobial efficacy on the wound. In addition, new epithelial tissue was observed in the Ser-Au@MMI$_{10}$-treated group on day 4, and the morphology of the newly formed epithelial tissue was similar to normal skin on day 12, suggesting that Ser-Au@MMI$_{10}$ could promote wound healing.

In the *P. aeruginosa* infection model (Figure 9B), the wounds in the PBS-treated group were observed to have an epithelial loss and a large number of inflammatory cells on days 4 and 8, suggesting that the wound had a severe inflammatory response, whereas a small number of inflammatory cells and newly formed squamous epithelium were observed in the Ser-Au@MMI$_{10}$-treated group on day 8. In addition, the new epithelial tissue in the Ser-Au@ MMI$_{10}$-
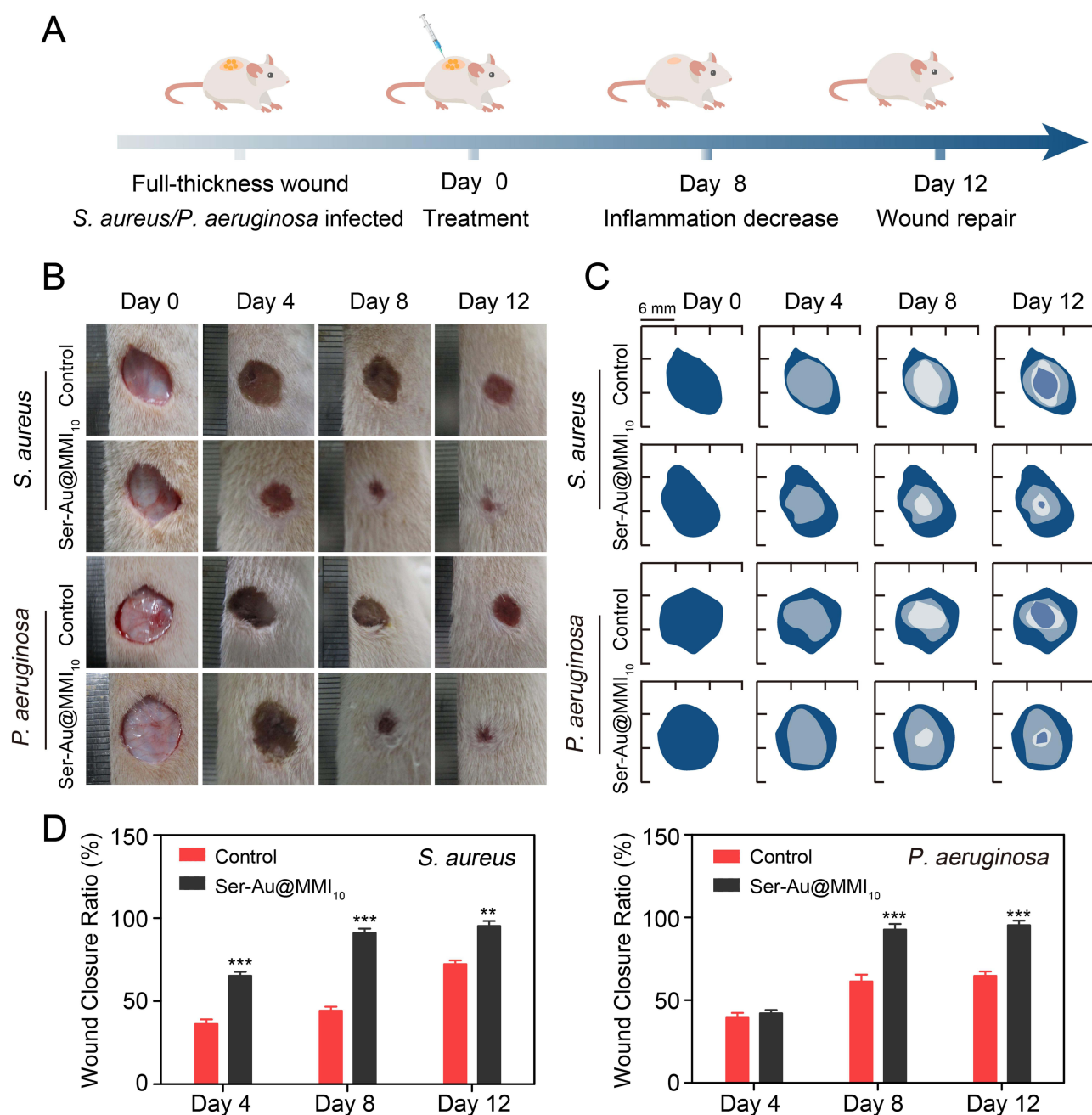
Figure 8 In vivo evaluation of the therapeutic effect of Ser-Au@MMI$_{10}$ after wound infection with *S. aureus* or *P. aeruginosa* in SD rats. (**A**) Schematic of the establishment of a full-thickness wound infected with *S. aureus* or *P. aeruginosa* and treatment with Ser-Au@MMI$_{10}$. (**B**) Wound healing photographs and (**C**) schematic of healing sites at days 0, 4, 8, and 10. (**D**) Wound healing rates of *S. aureus*-infected wounds or *P. aeruginosa*-infected wounds after Ser-Au@MMI$_{10}$ treatment.

treated group was similar to the normal skin epidermis on day 12. These results indicate that Ser-Au@MMI$_{10}$ has excellent antimicrobial properties and accelerates the healing of infected wounds.

Conclusion

In this study, we synthesized Ser-Au NPs using sericin as reducing and stabilizing agents, which exhibited excellent colloidal stability at different pH and salt concentrations, attributed to the fact that sericin wrapped around the outside of the gold nanoparticles prevented the aggregation of the particles through spatial repulsion. Subsequently, Ser-Au NPs were employed as a delivery system loaded with a small drug molecule (MMI) to investigate biocompatibility and
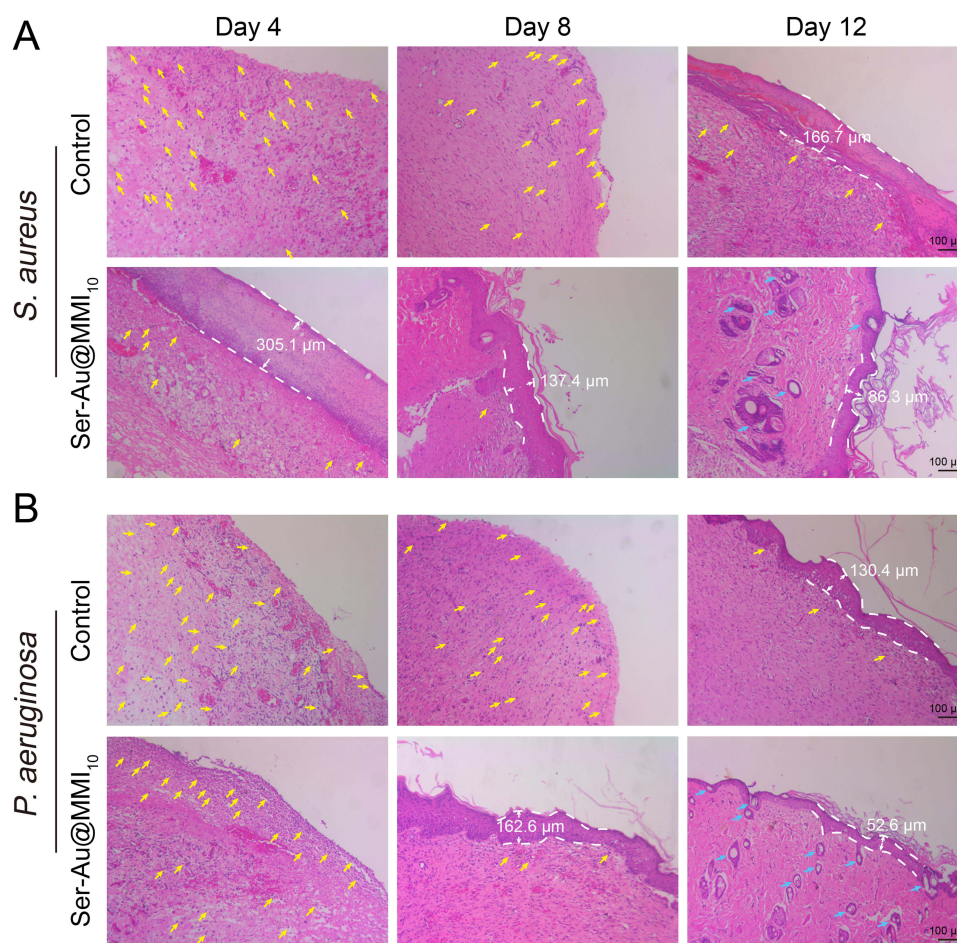
Figure 9 H&E staining of the full-skin wound on days 4, 8, and 12. (**A**) *S. aureus*-infected wounds and (**B**) *P. aeruginosa*-infected wounds after Ser-Au@MMI$_{10}$ treatments. Inflammatory cells are marked with yellow arrows; Epithelial borders are marked with white dotted lines.

antimicrobial efficacy. Due to the synergistic effect of MMI and AuNP, Ser-Au@MMI$_{10}$ has excellent antimicrobial properties. Its antimicrobial mechanism is that it breaks down bacteria's cell walls, destroying their structural integrity. In addition, we found that Ser-Au@MMI$_{10}$ could effectively disrupt the bacterial biofilm and kill bacteria at a low concentration (64 μg/mL). However, there was no significant cytotoxicity against L929 cells. Moreover, in vivo animal experiments have shown that Ser-Au@MMI$_{10}$ accelerated infected wound healing. Our findings suggest that Ser-Au @MMI has great potential for application in anti-biofilms and treating bacterial infections.

Acknowledgments

Disclosure

The authors declare that they have no known competing financial interests or personal relationships that could have appeared to influence the work reported in this paper.

References

1. Zhang S, Yang H, Wang M. et al. Immunomodulatory biomaterials against bacterial infections: progress, challenges, and future perspectives. *Innovation*. 2023;4(6):100503. doi:10.1016/j.xinn.2023.100503

2. Stewart PS, Bjarnsholt T. Risk factors for chronic biofilm-related infection associated with implanted medical devices. *Clin Microbiol Infect*. 2020;26(8):1034–1038. doi:10.1016/j.cmi.2020.02.027

3. Burden B, Rodriguez-Alvarez JS, Levi N, Gayzik FS. Application of survival analysis to model proliferation likelihood of biofilm following laser-induced hyperthermia treatment. *Front Bioeng Biotechnol*. 2023;11:1001017.

4. Mei JW, Xu DD, Wang LT, et al. Biofilm microenvironment-responsive self-assembly nanoreactors for all-stage biofilm associated infection through bacterial cuproptosis-like death and macrophage re-rousing. *Adv Mater*. 2023;35(36):2303432. doi:10.1002/adma.202303432

5. Caldara M, Belgiovine C, Secchi E, Rusconi R. EnvironmentalMicrobiological, and immunological features of bacterial biofilms associated with implanted medical devices. *Clin Microbiol Rev*. 2022;35(2):e00221–20. doi:10.1128/cmr.00221-20

6. Gomaa HH, Amin DY, Ahmed AR, Ismail NA, El Dougdoug KA, Abd-Elhalim BT. Antimicrobial, antibiofilm, and antiviral investigations using Egyptian Phoenix dactylifera L. pits extract. *AMB Express*. 2024;14(1):44. doi:10.1186/s13568-024-01695-3

7. Zhao AL, Sun JZ, Liu YP. Understanding bacterial biofilms: from definition to treatment strategies. *Front Cell Infect Microbiol*. 2023;13:1137947. doi:10.3389/fcimb.2023.1137947

8. Li YR, Xing Z, Wang SC, Wang YL, Wang ZZ, Dong L. Disruption of biofilms in periodontal disease through the induction of phase transition by cationic dextrans. *Acta Biomater*. 2023;158:759–768. doi:10.1016/j.actbio.2023.01.008

9. Oliveira IM, Gomes M, Gomes LC, Pereira MFR, Soares OS, Mergulhao FJ. Performance of graphene/polydimethylsiloxane surfaces against and single- and dual-species biofilms. *Nanomaterials*. 2022;12(3):355. doi:10.3390/nano12030355

10. Tuon FF, Suss PH, Telles JP, Dantas LR, Borges NH, Ribeiro VST. Antimicrobial Treatment of Biofilms. *Antibiotics-Basel*. 2023;12(1):87. doi:10.3390/antibiotics12010087

11. Rumbaugh KP, Sauer KJNRM. Biofilm dispersion. *Nat Rev Microbiol*. 2020;18(10):571–586. doi:10.1038/s41579-020-0385-0

12. Zhou L, Zheng H, Liu ZX, et al. Conductive antibacterial hemostatic multifunctional scaffolds based on $Ti_3C_2T_x$ MXene nanosheets for promoting multidrug-resistant bacteria-infected wound healing. *Acs Nano*. 2021;15(2):2468–2480. doi:10.1021/acsnano.0c06287

13. Guo Y, Xie B, Jiang M, et al. Facile and eco-friendly fabrication of biocompatible hydrogel containing CuS@ Ser NPs with mechanical flexibility and photothermal antibacterial activity to promote infected wound healing. *J Nanobiotechnol*. 2023;21(1):266. doi:10.1186/s12951-023-02035-6

14. Abdelhai MF, Shabaan RH, Kamal NM, Elemary EA, Abd-Elhalim BT, Hassan EA. Copper nanoparticles biosynthesis by Stevia rebaudiana extract: biocompatibility and antimicrobial application. *AMB Express*. 2024;14(1):59. doi:10.1186/s13568-024-01707-2

15. Cui F, Li T, Wang D, Yi S, Li J, Li X. Recent advances in carbon-based nanomaterials for combating bacterial biofilm-associated infections. *J Hazard Mater*. 2022;431:128597. doi:10.1016/j.jhazmat.2022.128597

16. Blanco-Cabra N, Alcàcer-Almansa J, Admella J, Arévalo-Jaimes BV, Torrents E. Nanomedicine against biofilm infections: a roadmap of challenges and limitations. *Wiley Interdisciplin Rev-Nanomed Nanobiotechnol*. 2024;16(1):e1944. doi:10.1002/wnan.1944

17. Mohamed SH, Othman BA, Abd-Elhalim BT, Seada MNA. Copper nanoparticles biosynthesis by Priestia megaterium and its application as antibacterial and antitumor agents. *Sci Rep*. 2024;14(1):23615. doi:10.1038/s41598-024-72598-3

18. Shabbir M, Atiq A, Wang J, et al. Metal-coordinated amino acid/peptide/protein-based supramolecular self-assembled nanomaterials for anticancer applications. *Aggregate*. 2024;e672.

19. Saeed N, Atiq A, Rafiq F, et al. Engineering of self-assembled silver-peptide colloidal nanohybrids with enhanced biocompatibility and antibacterial activity. *Sci Rep*. 2024;14(1):26398. doi:10.1038/s41598-024-78320-7

20. Li SL, Jiang M, Zhang Y, et al. Multi-functional carboxymethyl chitosan/sericin protein/halloysite composite sponge with efficient antibacterial and hemostatic properties for accelerating wound healing. *Int J Biol Macromol*. 2023;234:123357. doi:10.1016/j.ijbiomac.2023.123357

21. Fang J, Wan Y, Sun Y, et al. Near-infrared-activated nanohybrid coating with black phosphorus/zinc oxide for efficient biofilm eradication against implant-associated infections. *Chem Eng J*. 2022;435:134935. doi:10.1016/j.cej.2022.134935

22. Rokicka P, Markowska-Szczupak A, Kowalczyk L, Kowalska E, Morawski AW. Influence of titanium dioxide modification on the antibacterial properties. *Pol J Chem Technol*. 2016;18(4):56–64. doi:10.1515/pjct-2016-0071

23. Baig U, Ansari MA, Gondal MA, Akhtar S, Khan FA, Falath WS. Single step production of high-purity copper oxide-titanium dioxide nanocomposites and their effective antibacterial and anti-biofilm activity against drug-resistant bacteria. *Mater Sci Eng C-Mater Biol Appl*. 2020;113:110992. doi:10.1016/j.msec.2020.110992

24. Guo QQ, Zhao Y, Dai XM, et al. Functional silver nanocomposites as broad-spectrum antimicrobial and biofilm-disrupting agents. *ACS Appl Mater Interfaces*. 2017;9(20):16835–16848.

25. Xiong PZ, Huang XM, Ye NJ, et al. Cytotoxicity of metal-based nanoparticles: from mechanisms and methods of evaluation to pathological manifestations[J]. *Adv Sci*. 2022;9(16):2106049. doi:10.1002/advs.202106049

26. Ouyang J, Bu QY, Tao N, et al. A facile and general method for synthesis of antibiotic-free protein-based hydrogel: wound dressing for the eradication of drug-resistant bacteria and biofilms. *Bioact Mater*. 2022;18:446–458. doi:10.1016/j.bioactmat.2022.03.033

27. Persaud I, Raghavendra AJ, Paruthi A, et al. Defect-induced electronic states amplify the cellular toxicity of ZnO nanoparticles. *Nanotoxicology*. 2020;14(2):145–161. doi:10.1080/17435390.2019.1668067

28. Wang Y, Chu TD, Jin T, et al. Cascade reactions catalyzed by gold hybrid nanoparticles generate CO gas against periodontitis in Diabetes. *Adv Sci*. 2024;11(24):2308587. doi:10.1002/advs.202308587

29. Sadeghi S, Agharazi F, Hosseinzadeh SA, et al. Gold nanoparticle conjugation enhances berberine's antibacterial activity against methicillin-resistant (MRSA). *Talanta*. 2024;268:125358. doi:10.1016/j.talanta.2023.125358

30. Wang L, Natan M, Zheng WS, et al. Small molecule-decorated gold nanoparticles for preparing antibiofilm fabrics. *Nanoscale Adv*. 2020;2 (6):2293–2302. doi:10.1039/D0NA00179A

31. Yeh YC, Creran B, Rotello VM. Gold nanoparticles: preparation, properties, and applications in bionanotechnology. *Nanoscale*. 2012;4 (6):1871–1880. doi:10.1039/C1NR11188D

32. Sathishkumar M, Pavagadhi S, Mahadevan A, Balasubramanian R. Biosynthesis of gold nanoparticles and related cytotoxicity evaluation using A549 cells. *Ecotoxicol Environ Saf*. 2015;114:232–240. doi:10.1016/j.ecoenv.2014.03.020

33. Pinilla-Torres AM, Sanchez-Dominguez CN, Basilio-Bernabe K, et al. Green synthesis of Mesquite-gum-stabilized gold nanoparticles for biomedical applications: physicochemical properties and biocompatibility assessment. *Polymers*. 2023;15(17):3533. doi:10.3390/polym15173533

34. Zhang MW, Shao SX, Yue HT, et al. High Stability Au NPs: from design to application in nanomedicine. *Int J Nanomed*. 2021;16:6067–6094. doi:10.2147/IJN.S322900

35. Zhang DJ, You HJ, Zhang LL, Fang JX. Facile surface modification of mesoporous au nanoparticles for highly sensitive SERS detection. *Anal Chem*. 2020;92(23):15379–15387. doi:10.1021/acs.analchem.0c02781

36. Elbert KC, Jishkariani D, Wu Y, Lee JD, Donnio B, Murray CB. Design, self-assembly, and switchable wettability in hydrophobic, hydrophilic, and janus dendritic ligand–gold nanoparticle hybrid materials. *Acta Biomater*. 2017;29(20):8737–8746.

37. Ahmad S, Ahmad S, Ali S, Esa M, Khan A, Yan H. Recent advancements and unexplored biomedical applications of green synthesized Ag and Au nanoparticles: a review. *Int J Nanomed*. 2024;19:3187–3215. doi:10.2147/IJN.S453775

38. Yosri N, Khalifa SAM, Guo ZM, Xu BJ, Zou XB, El-Seedi HR. Marine organisms: pioneer natural sources of polysaccharides/proteins for green synthesis of nanoparticles and their potential applications. *Int J Biol Macromol*. 2021;193:1767–1798. doi:10.1016/j.ijbiomac.2021.10.229

39. Yuan LL, Jiang XY, Jiang M, et al. Biocompatible gellan gum/sericin hydrogels containing halloysite@polydopamine nanotubes with hemostasis and photothermal antibacterial properties for promoting infectious wound repair. *Mater Des*. 2023;227:111744. doi:10.1016/j.matdes.2023.111744

40. Li WL, Wu ZD, Zhao JY, et al. Fabrication of dual physically cross-linked polyvinyl alcohol/agar hydrogels with mechanical stability and antibacterial activity for wound healing. *Int J Biol Macromol*. 2023;247:125652. doi:10.1016/j.ijbiomac.2023.125652

41. Ming P, Liu Y, Yu P, et al. A biomimetic Se-nHA/PC composite microsphere with synergistic immunomodulatory and osteogenic ability to activate bone regeneration in periodontitis. *Small*. 2024;20(9):2305490.

42. Jiang M, Li SL, Ming PY, et al. Rational design of porous structure-based sodium alginate/chitosan sponges loaded with green synthesized hybrid antibacterial agents for infected wound healing. *Int J Biol Macromol*. 2023;237.

43. Ming PY, Rao PC, Wu TL, et al. Biomimetic design and fabrication of sericin-hydroxyapatite based membranes with osteogenic activity for periodontal tissue regeneration. *Front Bioeng Biotechnol*. 2022;10:899293. doi:10.3389/fbioe.2022.899293

44. Tian L, Wang XY, Zhang D, et al. Evaluation of the membrane damage mechanism of protocatechualdehyde against and simulation of growth inhibition in pork. *Food Chem*. 2021;363:130340. doi:10.1016/j.foodchem.2021.130340

45. Jiang X, Yuan L, Ming P, et al. Muscle-inspired lamellar chitosan sponge with photothermal antibacterial and antioxidant properties for hemostasis and accelerated bacteria infected wound healing. *Appl Mater Today*. 2023;35:101992. doi:10.1016/j.apmt.2023.101992

46. Tao G, Cai R, Wang YJ, et al. Bioinspired design of AgNPs embedded silk sericin-based sponges for efficiently combating bacteria and promoting wound healing. *Mater Des*. 2019;180:107940. doi:10.1016/j.matdes.2019.107940

47. Jia L, Guo L, Zhu JX, Ma YL. Stability and cytocompatibility of silk fibroin-capped gold nanoparticles. *Mater Sci Eng C-Mater Biol Appl*. 2014;43:231–236. doi:10.1016/j.msec.2014.07.024

48. Yilmaz B, Pazarceviren AE, Tezcaner A, Evis Z. Historical development of simulated body fluids used in biomedical applications: a review. *Microchem J*. 2020;155:104713. doi:10.1016/j.microc.2020.104713

49. Koeppel A, Laity PR, Holland CJAB. The influence of metal ions on native silk rheology. *Acta Biomater*. 2020;117:204–212. doi:10.1016/j.actbio.2020.09.045

50. Muindi MP, Lee JH, Kweon H, Kasina M. Effect of extraction ingredients on the conformation and stability of silk sericin (SS). *Polymers*. 2022;14(19):4118. doi:10.3390/polym14194118

51. Qin NQ, Wu XY, Liu XX, et al. Well-arranged hollow Au@Zn/Ni-MOF-2-NH core-shell nanocatalyst with enhanced catalytic activity for biomass-derived D-xylose oxidation. *ACS Sustainable Chem Eng*. 2022;10(17):5396–5403. doi:10.1021/acssuschemeng.1c07977

52. Lu BT, Lu F, Ran LX, et al. Imidazole-molecule-capped chitosan-gold nanocomposites with enhanced antimicrobial activity for treating biofilm-related infections. *J Colloid Interface Sci*. 2018;531:269–281. doi:10.1016/j.jcis.2018.07.058

53. Zhu Y, Chen P, Hu B, et al. MDSC-targeting gold nanoparticles enhance PD-1 tumor immunotherapy by inhibiting NLRP3 inflammasomes. *Biomaterials*. 2024;307:122533. doi:10.1016/j.biomaterials.2024.122533

54. Arciola CR, Campoccia D, Speziale P, Montanaro L, Costerton JW. Biofilm formation in implant infections. A review of molecular mechanisms and implications for biofilm-resistant materials. *Biomaterials*. 2012;33(26):5967–5982. doi:10.1016/j.biomaterials.2012.05.031